JPET Fast Forward. Published on January 8, 2019 as DOI: 10.1124/jpet.118.252858
This article has not been copyedited and formatted. The final version may differ from this version.

Title Page

Measurement and Quantitative Characterization of Whole-Body Pharmacokinetics of Exogenously Administered T Cells in Mice

Antari Khot[1], Satoko Matsueda[2], Veena A. Thomas[1,3], Richard C. Koya[2], and Dhaval K. Shah[1,*]

[1] Department of Pharmaceutical Sciences, School of Pharmacy and Pharmaceutical Sciences, The State University of New York at Buffalo, Buffalo, NY 14214, USA

[2] Center for Immunotherapy, Roswell Park Cancer Institute, Buffalo, NY 14263, USA

[3] V.A.T is currently employed at Department of Pharmacokinetics and Drug Metabolism, Amgen Inc., South San Francisco, CA, USA

Running Title Page

Running Title: Whole-Body PK and PBPK Model for T cells

*Corresponding author:
Dhaval K. Shah, PhD
Department of Pharmaceutical Sciences
455 Kapoor Hall, School of Pharmacy and Pharmaceutical Sciences
State University of New York at Buffalo
Buffalo, New York 14214
Phone: 716-645-4819
Email: dshah4@buffalo.edu

Number of Text Pages: 28
Number of Tables: 2
Number of Figures: 5 (4 main + 1 supplementary)
Number of References: 44
Number of words in Abstract: 250
Number of words in Introduction: 861
Number of words in Discussion: 1811

List of Abbreviations:

TCR-T cells – T cell receptor modified T cells, CAR-T cells – chimeric antigen receptor T cells, TILs - tumor infiltrating lymphocytes, AUC - area under the concentration-time curve, BC - biodistribution coefficient, %ID/g – percent of injected dose per gram of tissue, Cr-51 – chromium-51, I-125 – Iodine-125, In-111 – Indium-111, TDLN – tumor draining lymph node, IGLN – inguinal lymph node, TDL – thoracic duct lymphocytes, PK – pharmacokinetics, PBPK model – physiologically based pharmacokinetic model

ABSTRACT

Here we have investigated whole-body pharmacokinetics (PK) of exogenously administered T cells in a mouse model of melanoma, and have development of a physiologically based pharmacokinetic (PBPK) model to quantitatively characterize the data. T cells were isolated from the spleen of tumor-bearing mice, activated, and labeled with Cr-51 to facilitate the quantification. Labeled T cells were injected in the tumor-bearing mice and PK was measured in 19 different tissues. It was found that T cells disappear from the blood rapidly after administration, and accumulate in the tissues to various extent. Spleen, liver, lung, kidney, bone, and lymph nodes accounted for more than 90% of T cells in the body. The distribution of T cells in solid tumor was found to be very low, hovering below 1 %ID/g during the entire study. However, this observation may differ for targeted TCR-T and CAR-T cells. Observed PK profiles also suggest that T cell based therapies may be more successful in treating cancers of the lymphatic system and bone marrow metastases compared to solid tumors. A PBPK model was developed to characterize the whole-body PK of T cells, which incorporated key processes like extravasation, elimination, and recirculation of T cells via lymph flow. Retention factors were incorporated into spleen, liver, and kidney to adequately capture the PK profiles. The model was able to characterize observed PK profiles reasonably well, and parameters were estimated with good confidence. The PK data and PBPK model presented here provides unprecedented insight into biodistribution of exogenously administered T cells.

INTRODUCTION

Adoptive cell therapy (ACT) has been gaining interest over the past three decades as a targeted anticancer therapy. Several advancements have been made in this field, which include tumor infiltrating lymphocytes (TILs) and engineered cells like T cell receptor T cells (TCR-T) and chimeric antigen receptor T cells (CAR-T). In fact, CAR-T cells targeting more than 25 tumor antigens have been investigated in preclinical and clinical studies so far, resulting in recent approvals of Kymriah™ and Yescarta™ for the treatment of hematologic cancers like B cell leukemia and lymphoma (Gross and Eshhar, 2016). However, the development of T cell based therapies for solid tumors remains challenging for several reasons, such as unknown cellular trafficking to the site-of-action, inadequate tumor infiltration, and immunosuppressive tumor microenvironment (Newick et al., 2017; Xia et al., 2017). In addition, despite the clinical success, to date we do not have a comprehensive understanding about the whole body pharmacokinetics (PK) of T cell based therapeutics. Since T cells possess unique properties like tissue margination, the PK of T cells is bound to be different than traditional small or large molecules, and requires further investigation to understand and predict the exposure-response relationships for the efficacy and toxicity of T cell based therapeutics.

There are only few published studies that have investigated the elimination and biodistribution of T cells in various tissues of mice (Table 2). These studies have been limited in the number of sampling time points and the tissues being analyzed, and provide contradictory results. Wallace *et al*. were amongst the first to investigate the disposition of I-125-PKH95 labeled TILs and activated splenocytes in MC38 lung metastases bearing mice (Wallace et al., 1993). They

observed that 20 hours after the administration, activated splenocytes accumulated more in the spleen followed by lung and liver, whereas the TILs accumulated more in the lungs followed by spleen and liver. Interestingly, the authors concluded that higher retention of TILs in the lungs was not because of the presence of lung metastases as a similar disposition pattern was also observed for non-tumor bearing mice. Melder *et al*. subsequently presented a more comprehensive investigation, where tumor-antigen activated and normal (non-activated) lymphocytes obtained from the spleen were labeled with the residualizing isotope Indium-111, and the PK of the cells was measured in MCaIV mammary carcinoma bearing mice (Melder et al., 2002). They observed that the PK of tumor antigen activated and normal lymphocytes was the same, and the specificity of the lymphocytes towards the tumor antigen did not result in a significant increase in tumor uptake. They also found that the spleen and the liver were the major tissues that demonstrated lymphocyte accumulation. However, more recently Xu *et al*. used CFSE labeled $CD3^+$ T cells that were derived from mouse spleen and activated against tumor antigen, and concluded that 1-3 days after administration the T cells accumulate to a high level in the tumor followed by liver, kidney, and spleen (Xu et al., 2013). As such, the extent of T cell distribution in many tissues is not known and there is not a consensus on the expected PK profiles of exogenously administered T cell therapeutics throughout the body.

In addition, there is also a lack of robust mathematical models that can accurately describe the whole-body PK of T cell. Most of the models developed so far are based on scant biodistribution data. Stekel *et al*. and Ganusov *et al*. have developed minimal PBPK models to describe T cell disposition in rats (Stekel et al., 1997; Ganusov and Auerbach, 2014). The model by Stekel *et al*. includes blood, spleen and lymphatic compartments, and the model by Ganusov *et al*. includes

blood, lung, liver, spleen, peyer's patch, mesenteric, and subcutaneous lymph node compartments. More comprehensive models have been developed by Zhu *et al*. for mouse, rat, and human (Zhu et al., 1996). Their model includes most of the tissues and tumor, and each tissue compartment is divided into vascular and extravascular spaces to account for rolling, adhesion, and extravasation of T cells in tissues. However, these models are based on very sparse data from 2-3 tissues in each species, and many parameters of the model were fixed to zero due to the lack of experimental data.

In order to better understand whole-body PK of exogenously administered T cells, and to facilitate the development of a more reliable and robust mathematical model, here we have presented a comprehensive PK investigation in a mouse model of melanoma. T cells were isolated from mouse spleen, activated, and labeled with Cr-51, which is reported to be a reliable label with no significant elution from the cells or reuptake into other cells (McMillan and Scott, 1968; Rannie and Donald, 1977). In fact, labeling lymphocytes with Cr-51 to investigate their in vivo biodistribution is an old and well-established method (Zatz and Lance, 1970). Labelled T cells were injected into tumor-bearing mice, and the PK of T cells was measured in blood, tumor, and tissues. Measured PK profiles were quantitatively characterized using a novel PBPK model developed for exogenously administered T cells. Observed PK profiles were also compared with previously reported results.

METHODS

Reagents, cell line, and animal

Mouse melanoma cell line B16-BL6 was obtained from Creative Bioarray, and maintained in DMEM medium with 10% heat inactivated fetal bovine serum and 1% penicillin-streptomycin. Cells were cultured at 37°C in 5% CO_2 in a humidified incubator. All animal experiments were performed in accordance with the protocols approved by Institutional Animal Care and Use Committee (IACUC). Eight-weeks-old male C57BL/6 mice were purchased from Taconic Biosciences and housed individually. Mice were subcutaneously inoculated with 0.5 million B16-BL6 cells to develop the tumor. When the tumor volume reached ~250 mm^3, mice were subjected to the experimental procedure below. Sodium chromate (1 mCi/ml of ^{51}Cr) was purchased from Perkin-Elmer Inc., and anti-CD3 and anti-CD28 antibodies were purchased from BD Biosciences. Reagents for TIL isolation such as mouse tumor dissociation kit, anti-CD105 antibody-biotin, anti-CD3 antibody-biotin, anti-biotin microbeads ultrapure, LD columns, LS columns, QuadroMACS™ separator were purchased from Miltenyi Biotec.

Isolation and expansion of T cells from mouse spleen

Spleen from a melanoma-bearing mouse was collected and homogenized under aseptic conditions, to obtain a mononuclear cell suspension in AIM V medium containing 10% FBS and beta-mercaptoethanol. Cell suspension was centrifuged at 400 g and re-suspended in RBC lysis buffer for 5 minutes at room temperature. AIM V medium was added to dilute lysis buffer and centrifuged to remove the buffer and medium, followed by resuspension of the pellet in AIM V medium at a density of 1-2 x 10^7 cells/ml in a non-tissue culture treated flask. The flask was pre-coated with 1 µg/ml anti-CD3 and anti-CD28 antibodies in 5 ml of PBS overnight at 4°C. PBS

solution containing antibodies was removed before adding mononuclear cell suspension. IL-2 at a concentration of 50 IU/ml was added to cell suspension in the flask. After 48 h, cells were centrifuged and media was replaced by fresh AIM V media with IL-2. Four days after isolation of splenocytes the cells were analyzed using flow cytometer to determine the expression of CD3 and CD8. (Trickett and Kwan, 2003; Koya et al., 2012)

Isolation of tumor infiltrating lymphocytes

To facilitate a pilot study, TILs were isolated for mouse melanoma tumors using paramagnetic bead system. Melanoma tumors were processed using the tumor dissociation kit to generate a single cell suspension of tumor cells. B16-BL6 cells were depleted from the slurry of cells by passing the cells labeled with biotin-anti-CD105 antibody and anti-biotin microbeads through the LD column. The T cells were then labeled for positive selection using biotin-anti-CD3 antibody and isolated using LS columns.

Cr-51 labeling and pharmacokinetic study

T cells collected from mouse spleen were washed with PBS and incubated with sodium chromate (0.5 mCi of Cr-51 for 200 x 10^6 cells) for 1 h at room temperature. After incubation, cells were washed three times with PBS to remove free Cr-51. Radioactivity of final cell suspension was measured using gamma counter. 10 µCi of labeled T cells were injected in melanoma-bearing mice via penile vein injections. Mice (n=3) were sacrificed at pre-determined time points (1 h, 1 day, 3, 7, and 14 days) and 19 tissues were collected from each mouse including blood, tumor, inguinal lymph nodes (tumor-draining (TDLN) and non-tumor draining (IGLN)), lungs, heart, kidney, spleen, liver, bone, muscle, skin, brain, thyroid, small intestine, large intestine, pancreas, adipose, and testicles. Above mentioned sampling times were chosen based on several factors.

While we wanted to investigate the biodistribution of T cells for more than 4 weeks, the tumor volume reached permissible IACUC limit within two weeks, and hence we had to design our study for only a period of 2 weeks. Although, we could have reduced the initial tumor volume to a value lower than ~200-250 mm^3 to prolong the study duration, it would have affected our ability to quantify T cells in the tumor, and hence it was not a viable option. Despite acceptable labeling efficiency, 10-20 million T cells were needed to be injected per animal to attain radioactive dose of 10 µCi, hence we were restricted by the number of T cells available while choosing how many animals we can include in the study. Lastly, since most of the previous studies have reported T cell disposition for a short period of time, we wanted to make sure we include at least 2 early sampling time points (i.e. <24h) for comparison with published data, and enough time points later on to capture the elimination of T cells from the system.

Blood and tissues were collected in pre-weighed tubes and their radioactivity was measured using a gamma counter. Radioactive counts were corrected for background and decay. Final counts per minute were converted to percent of injected dose/gram of tissue (%ID/g) by using the following equation:

$$\frac{\%ID}{gram\ of\ tissue} = \frac{corrected\ cpm * 100}{injected\ cpm * weight\ of\ tissue\ in\ grams}.$$

PBPK model development

Figure 1 describes the PBPK model developed to characterize whole-body PK of T cells. The model includes 12 major tissues and a tumor compartment, connected in an anatomical manner via blood and lymph flows. All tissue compartments are divided into vascular and extravascular sub-compartments to characterize the process of T cell extravasation. Extravasation of T cells in each tissue is captured using an irreversible first-order transmigration rate process. For most of the

tissues it was assumed that the transmigrated T cells in the extravascular space recirculate back into the lymph nodes via the lymphatic flow. For bone and muscle it was assumed that half of the T cells recirculate to IGLN (left inguinal LN) and the rest recirculate to TDLN (right inguinal LN). Since tibia and thigh muscle were collected as representative bone and muscle tissues, to mimic the physiology of lymph drainage into the inguinal LN from hind legs, we divided the lymph flow from muscle and bone into right and left inguinal lymph nodes. Considering the tumor was implanted in the right flank, lymph drainage from the tumor was added only in the right inguinal LN (i.e. TDLN). Lymphatic fluid from all tissues was assumed to drain into lymph nodes, which were connected to the central blood compartment. To capture the T cell concentrations in IGLN and TDLN, the model incorporated two more transit lymph node compartments, which were assumed to receive lymphatic fluids from bone, muscle, and tumor. Elimination of T cells was assumed occur only in the vascular compartment of lungs, based on the model by Zhu *et al*. (Zhu et al., 1996). To capture the plateauing concentrations of T cell in spleen, liver, and kidney over the time, retention factors were incorporated into those tissues. To maintain the mass balance, "others" compartment was incorporated into the PBPK model. All the physiological parameters for the mouse PBPK model (i.e. blood and lymph flow values, and compartment volumes) were obtained from the literature (Shah and Betts, 2012). Blood flow for tumor compartment was obtained from Zhu *et al*. (Zhu et al., 1996) and total tumor volume was based on the average tumor size in our study. Transmigration rates of T cells for each tissue, and the retention factors, were estimated by fitting the model to observed whole-body PK data. The equations for the PBPK model are provided below, and the description of model parameters is provided in Table 1.

Model Equations

JPET Fast Forward. Published on January 8, 2019 as DOI: 10.1124/jpet.118.252858
This article has not been copyedited and formatted. The final version may differ from this version.

Whole blood

$$\frac{d}{dt}C_{whole\ blood} = (-(Q_{lung}+L_{lung})*C_{whole\ blood}+(Q_{heart}-L_{heart})*C_{heart}^{vascular}+(Q_{kidney}-L_{kidney})*C_{kidney}^{vascular}+(Q_{brain}-L_{brain})*C_{brain}^{vascular}+(Q_{muscle}-L_{muscle})*C_{muscle}^{vascular}+(Q_{bone}-L_{bone})*C_{bone}^{vascular}+(Q_{skin}-L_{skin})*C_{skin}^{vascular}+(Q_{adipose}-L_{adipose})*C_{adipose}^{vascular}+((Q_{SI}-L_{SI})+(Q_{LI}-L_{LI})+(Q_{spleen}-L_{spleen})+(Q_{pancreas}-L_{pancreas})+(Q_{liver}-L_{liver}))*C_{liver}^{vascular}+(Q_{others}-L_{others})*C_{others}^{vascular}+L_{lymph\ node}*C_{lymph\ node})/V_{whole\ blood} \quad (1)$$

Lungs

Vascular

$$\frac{d}{dt}C_{lung}^{vascular} = ((Q_{lung}+L_{lung})*C_{whole\ blood} - Q_{lung}*C_{lung}^{vascular} - J_{lung}*C_{lung}^{vascular}*V_{lung}^{vascular} - E_{lung}*C_{lung}^{vascular}*V_{lung}^{vascular})/V_{lung}^{vascular} \quad (2)$$

Extravascular

$$\frac{d}{dt}C_{lung}^{extravascular} = (J_{lung}*C_{lung}^{vascular}*V_{lung}^{vascular} - L_{lung}*C_{lung}^{extravascular}*F_{lung})/V_{lung}^{extravascular} \quad (3)$$

Typical Tissue

Vascular

$$\frac{d}{dt}C_{tissue}^{vascular} = (Q_{tissue}*C_{lung}^{vascular} - (Q_{tissue}-L_{tissue})*C_{tissue}^{vascular} - J_{tissue}*C_{tissue}^{vascular}*V_{tissue}^{vascular})/V_{tissue}^{vascular} \quad (4)$$

Extravascular

$$\frac{d}{dt}C_{tissue}^{extravascular} = (J_{tissue}*C_{tissue}^{vascular}*V_{tissue}^{vascular} - L_{tissue}*C_{tissue}^{extravascular}*F_{tissue})/V_{tissue}^{extravascular} \quad (5)$$

Tissues with retention factor

Vascular

$$\frac{d}{dt}C_{tissue}^{vascular} = (Q_{tissue}*C_{lung}^{vascular} - (Q_{tissue}-L_{tissue})*C_{tissue}^{vascular} - J_{tissue}*C_{tissue}^{vascular}*V_{tissue}^{vascular})/V_{tissue}^{vascular} \quad (6)$$

JPET Fast Forward. Published on January 3, 2019 as DOI: 10.1124/jpet.118.252858
This article has not been copyedited and formatted. The final version may differ from this version.

Extravascular

$$\frac{d}{dt}C_{tissue}^{extravascular} = (J_{tissue} * C_{tissue}^{vascular} * V_{tissue}^{vascular} - L_{tissue} * \frac{C_{tissue}^{extravascular}}{R_{tissue}} * F_{tissue}) / V_{tissue}^{extravascular} \quad (7)$$

Liver

Vascular

$$\frac{d}{dt}C_{liver}^{vascular} = (Q_{liver} * C_{lung}^{vascular} + (Q_{SI} - L_{SI}) * C_{SI}^{vascular} + (Q_{LI} - L_{LI}) * C_{LI}^{vascular} + (Q_{spleen} - L_{spleen}) * C_{spleen}^{vascular} + (Q_{pancreas} - L_{pancreas}) * C_{pancreas}^{vascular} - ((Q_{SI} - L_{SI}) + (Q_{LI} - L_{LI}) + (Q_{spleen} - L_{spleen}) + (Q_{pancreas} - L_{pancreas}) + (Q_{liver} - L_{liver})) * C_{liver}^{vascular} - J_{liver} * C_{liver}^{vascular} * V_{liver}^{vascular}) / V_{liver}^{vascular} \quad (8)$$

Extravascular

$$\frac{d}{dt}C_{liver}^{extravascular} = (J_{liver} * C_{liver}^{vascular} * V_{liver}^{vascular} - L_{liver} * \frac{C_{liver}^{extravascular}}{R_{liver}} * F_{liver}) / V_{liver}^{extravascular} \quad (9)$$

Lymph node

$$\frac{d}{dt}C_{lymph\ node} = (F_{lung} * L_{lung} * C_{lung}^{extravascular} + F_{heart} * L_{heart} * C_{heart}^{extravascular} + L_{kidney} * \frac{C_{kidney}^{extravascular}}{R_{kidney}} * F_{kidney} + F_{brain} * L_{brain} * C_{brain}^{extravascular} + C_{TDLN} * L_{TDLN} + C_{IGLN} * L_{IGLN} + F_{skin} * L_{skin} * C_{skin}^{extravascular} + F_{adipose} * L_{adipose} * C_{adipose}^{extravascular} + F_{SI} * L_{SI} * C_{SI}^{extravascular} + F_{LI} * L_{LI} * C_{LI}^{extravascular} + L_{spleen} * \frac{C_{spleen}^{extravascular}}{R_{spleen}} * F_{spleen} + F_{pancreas} * L_{pancreas} * C_{pancreas}^{extravascular} + L_{liver} * \frac{C_{liver}^{extravascular}}{R_{liver}} * F_{liver} + F_{others} * L_{others} * C_{others}^{extravascular} - L_{lymph\ node} * C_{lymph\ node}) / V_{lymph\ node} \quad (10)$$

Inguinal lymph node

$$\frac{d}{dt}C_{IGLN} = (Q_{bone} * (\frac{F_{bone}}{2}) * C_{bone}^{extravascular} + Q_{muscle} * (\frac{F_{muscle}}{2}) * C_{muscle}^{extravascular} - C_{IGLN} * Q_{IGLN}) / V_{IGLN} \quad (11)$$

Tumor draining lymph node

JPET Fast Forward. Published on January 8, 2019 as DOI: 10.1124/jpet.118.252858
This article has not been copyedited and formatted. The final version may differ from this version.

$$\frac{d}{dt} C_{TDLN} = (Q_{bone} * (\frac{F_{bone}}{2}) * C_{bone}^{extravascular} + Q_{muscle} * (\frac{F_{muscle}}{2}) * C_{muscle}^{extravascular} + F_{tumor} * L_{tumor} * C_{tumor}^{extravascular} - C_{TDLN} * Q_{TDLN}) / V_{TDLN} \quad (12)$$

PK analysis and PBPK model fitting

Area under the concentration vs. time curve (AUC) for all the T cell PK profiles and associated variability were calculated using non-compartmental analysis in Phoenix® WinNonlin® 7.0. The ratio of T cell AUC in the tissues over the AUC in the blood was represented as biodistribution coefficient (BC) value (Shah and Betts, 2013; Li et al., 2016). The PBPK model was fitted to observed PK data using the maximum likelihood estimation method of ADAPT V software (BMSR, CA). Following variance model was used for model fitting: Var(t)= $(\sigma_{intercept} + \sigma_{slope} Y(t))^2$, where $\sigma_{intercept}$ and σ_{slope} are variance model parameters and Y(t) is the model output.

RESULTS

Whole-body pharmacokinetics of T cells

Activation of splenocytes with anti-CD3 antibody, anti-CD28 antibody, and IL-2 led to more than 90% of $CD3^+$ T cells in the final preparation, of which >85% were $CD8^+$ cells. Representative flow cytometry analysis of these cells is provided in (Supplementary Figure 1). The efficiency of Cr-51 incorporation was ~50 µCi per 10^8 lymphocytes, and thus a dose of 10 µCi/mouse comprised of ~$2x10^7$ T cells administered per mouse. Figure 2 shows typical PK profiles generated following intravenous administration of Cr-51 labeled T cells in tumor-bearing mice, along with AUC values for each profile. It was found that T cells eliminated from the blood and the lungs rapidly within 24 hours, followed by their accumulation in spleen and liver. Smith *et al*. showed similar results in rats, where exogenous activated lymphocytes accumulated in lungs up to 4-6 hours and then localized to spleen and liver over 24 hours (Smith et al., 1980). This phenomenon can be attributed to the presence of reticuloendothelial system within spleen and liver, which is reported to be significantly involved in the disposition of T cells (Pabst, 1988; Norelli et al., 2016). In addition, lymphoid tissues such as lymph nodes and bone marrow also showed high accumulation of T cells over the time. Of note, no significant difference was seen between the PK of T cells in TDLN vs. IGLN (AUC: 635±77 vs. 712±192 %ID/g*h). Interestingly, T cell concentrations peaked around 24 h in the TDLN, which was similar to the tumor, whereas T cells accumulated gradually over 3-7 days in IGLN, which was similar to the bone marrow. Spleen, liver, lung, kidney, bone, and lymph nodes accounted for more than 90% of T cells in the body over the two weeks, with BC value of 448, 148, 39, 36, 27, and 16, respectively (Figure 2). The PK of T cell in the heart displayed similar profile as the lungs, where majority of the T cells eliminated

from the tissue by 72 hours. Intestines, pancreas, testes, muscle, fat, skin, and brain showed the lowest amount of T cell accumulation, with concentrations hovering below 0.5 %ID/g for most of the time. T cell concentrations in thyroid started of lower than 0.5 %ID/g, gradually decreased to below the limit of quantitation after three days, and two of three mice showed high T cell concentration on the day 14. This peculiar PK profile may stem from the lymphocytes that are recirculating back to the thyroid after two weeks, however this hypothesis needs further support. Importantly, tumor had a BC value of 1.3 and tumor concentrations of T cells hovered below 1 %ID/g during the whole study. This observation may stem from many factors, such as immunosuppressive tumor microenvironment, insufficient trafficking of T cells into the tumor, and lower tumor uptake of T cells due to less expression of cell adhesion molecules on the tumor cells (Pandolfi et al., 1992). Nonetheless, this data does bring into question the potential for treating solid tumors using T cell based therapy, and demands further investigation into the tumor disposition of targeted T cells like TCR-T and CAR-T cells. In addition, our results suggest that T cell based therapies may be more successful for treating cancers of the lymphatic system and bone marrow metastases.

Development of the T cell PBPK model

The PBPK model (Figure 1) was able to characterize T cell PK profiles in most of the tissues reasonably well (Figure 3). The model parameters were also estimated with good confidence (Table 1). The estimates of transmigration rates were higher for tissues showing high accumulation of T cells and BC values greater than 20, such as lung, spleen, liver and kidney. Retention factors for spleen, liver, and kidney were 9.8, 2.5 and 3.9, respectively. Incorporation of the retention process was necessary to characterize high concentrations of T cells in spleen

and liver, which may relate to T cell processing by the RES system. High concentrations of T cells in the kidney may stem from the presence of Cr-51 label in that organ. Elimination of T cells from the body was incorporated only in the lungs, and the parameter for this process was fixed to the value of 0.84 hr^{-1} obtained from Zhu *et al*. (Zhu et al., 1996). Of note, Zhu *et al*. had obtained this value by scaling down the parameter value estimated using the human data.

JPET Fast Forward. Published on January 8, 2019 as DOI: 10.1124/jpet.118.252858
This article has not been copyedited and formatted. The final version may differ from this version.

DISCUSSION

With the emergence of activated T cell and T cell targeting antibodies as novel anticancer therapeutics, it has become necessary to quantitatively understand the whole-body disposition of T cells, to further advance the clinical potential of these therapeutics. The process of T cell disposition is complex and depends on multiple stimuli-dependent steps like, rolling and adhesion on vascular endothelial cells, chemokine-driven extravasation, and margination to specific tissues (Hogg, 1993; Springer, 1994; Girard and Springer, 1995). This process is further complicated by dynamic regulation of cell adhesion molecules expressed on tissues and changes in cell surface phenotype based on the nature of the T cell (Defilippi et al., 1993; Ager et al., 2016). Nonetheless, as an important first step towards understanding the whole-body disposition of engineered T cells, here we have conducted a comprehensive PK study of activated T cells in a mouse model of melanoma. We have chosen a xenograft tumor model over spontaneous tumor model to avoid the possibility of developing host tolerance (Lechner et al., 2013). As such, further studies are warranted to assess how the T cell disposition may differ between xenograft, spontaneous, and orthotopic tumors.

The T cells employed in our investigation were isolated from the splenocytes of melanoma-bearing mice and expanded to enrich $CD3^+$ T cells. The cells were incubated with sodium chromate to accomplish Cr-51 labeling, and after the labeling >95% of cells were found to be alive via trypan blue method. An advantage of using Cr-51 as a label is the fact that Cr^{3+} ions bind to organic ions such as citrate and amino acids within the cells to form complexes, which do not leak out of the cells or nonspecifically transfer to surrounding cells (Sanderson, 1976). However, occasionally macrophages may phagocytose dead/dying T cells and accumulation small amount

of Cr-51, which should be kept in mind while interpreting the biodistribution data from Cr-51 labelled T cells (Sprent, 1976; Thakur, 2013).

Our findings were comparable to previously published sparse PK data (Table 2). Figure 4 shows the comparison of our PK data generated using Cr-51 labeled activated T cells, with previously published PK data generated using In-111 and I-125 labeled T cells (Wallace et al., 1993; Melder et al., 2002). We have also included data from a pilot PK study that was conducted using Cr-51 labeled TILs for comparison. This study was limited due to very low number of TILs available from B16-BL6 tumors, and PK data was collected only up to 24 hours. As shown in Figure 4, all the studies demonstrate that spleen has the highest accumulation of T cells followed by the liver. However, it was observed that T cells eliminated faster from the lungs, heart, and tumor in our study compared to In-111 labeled T cell study. This may be due to the residualizing nature of In-111, as the naïve and tumor antigen activated T cells demonstrated no difference in the PK profile. Interestingly, when TILs were administered, higher concentration of T cells was observed in the lungs compared to the spleen. This observation was similar to the one reported using I-125 labeled TILs (Melder et al., 2002), where lung had higher accumulation of tumor sensitized T cells compared to normal lymphocytes. This suggests that when T cells are activated against tumor antigens they may exhibit a tendency to accumulate in the lungs at a higher level. Although the mechanism for this phenomenon is not fully elucidated, there is an increase in LFA-1 clustering on TILs and their affinity towards ICAM-1, expressed in lungs, is also high, leading to higher accumulation of TILs in lungs (Hamann et al., 2000; Reina and Espel, 2017). Regardless of activation, lymphocytes are also known to temporarily accumulate in the lungs due to pressure difference between right ventricle that pumps the blood to the lungs and left ventricles that

circulates the blood through the rest of the body. During the long transit through the lung, lymphocytes can get trapped and exposed to alveolar macrophages, which can phagocytose small fraction of the cells (Hall, 1985; Westermann et al., 2003). Of note, in our study the tumor distribution of TILs was not much different than activated T cells. However, this observation needs further research using targeted TCR-T and CAR-T cells that can recognize tumor cells. In addition, we have only focused on quantitatively understanding the biodistribution of a pooled $CD3^+$ T cell population. Consequently, biodistribution characteristics of specific T cell subtypes may differ. It also remains to be investigated if the disposition of T cells throughout the body will be different between tumor-bearing and non-tumor bearing mice.

Other than mice, there are a few short-term lymphocyte migration studies reported in rats using chromium. Interestingly, these studies were conducted by labeling thoracic duct lymphocytes (TDLs) to track the recirculation of lymphocytes, which showed highest distribution in superficial lymph nodes within a day. Spleen was the second highest organ to exhibit accumulation, and the rest of the lymphoid and non-lymphoid tissues showed similar pattern as our study (Rannie and Donald, 1977; Smith and Ford, 1983; Ganusov and Auerbach, 2014). Smith *et al*., passaged the Cr-51 labeled thoracic duct lymphocytes through an intermediate animal before injecting them into final recipient rats, to mimic physiological conditions and reduce the effect of cell handling during in vitro incubation. Passaged TDLs entered and exited the spleen at a faster rate compared to non-passaged TDLs. Discrepancies such as this could stem from differences in the origin and maturation stage of the cells, cell handling procedures, or animal species used for the investigation, and may require further investigation (Bainbridge et al., 1966; Heslop and Hardy, 1971; Hamann et al., 2000).

When it comes to the evaluation of whole body disposition of lymphocytes in the humans, there is not much published except two studies conducted using chromium labeled lymphocytes (McMillan and Scott, 1968; Hersey, 1971). These studies were performed half a century ago, and the techniques used for isolation and expansion of lymphocytes from PBMCs were archaic. Nonetheless, McMillan and Scott reported high body surface counts of lymphocytes in the liver, followed by heart, spleen, and lung over the 24 hours. In addition, lymphocytes disappeared from the blood rapidly and very low Cr-51 counts were detectable 6 hours after the injection. However, Hersey followed lymphocyte distribution over 8 days in healthy and CLL patients, and reported high body surface counts in spleen, bone marrow, and liver. He concludes that the difference between his results and study performed by McMillan and Scott was the fact that earlier study was performed using mixture of leukocytes due to poor separation techniques. Hersey also observed that lymphocyte percent decreases fast from blood and lungs in healthy patients similar to earlier reports. Thus, it seems that both in humans and in mice lymphocytes distributes rapidly to the tissues immediately after the administration, where spleen and liver accumulates majority of the administered dose.

In this manuscript, we have also presented the development of a PBPK model to characterize whole-body PK of exogenously administered T cells. Our PBPK model is more parsimonious than previously published models (Zhu et al., 1996; Stekel et al., 1997; Ganusov and Auerbach, 2014), and developed based on dense PK data we have generated in this investigation. The PBPK model assumes retention of T cells in spleen, liver, and kidney, and elimination through only lungs. The retention phenomenon is incorporated using the retention factors, and it is based on several observations. It is reported that lymphocytes activated in vitro or in vivo tend to localize to

secondary lymphoid organs such as spleen (Gowans and Knight, 1964; Hamann and Rebstock, 1993), and we have observed as similar trend in our exogenous T cell PK study. Previous reports also suggest a slow turn-over and very long half-life of T cell subsets in certain tissues (Sprent and Tough, 1994), which may be the reason for the observed stable concentrations of T cells in spleen and liver over the time. As such, the retention factor in the model represents lymphocytes accumulation in the extravascular region of spleen, liver and kidney, which may stem from decreased recycling of lymphocytes from these tissues via the lymph flow. Elimination of T cells from the body was incorporated only in the lungs, based on the reports that T cells undergo relatively faster clearance in the lungs due to the presence of alveolar macrophages (Milik et al., 1997). However, it is important to note that estimated value of pulmonary clearance for the T cells may be inflated, as the model do not take into account elimination of T cells from tissues like liver and spleen, which have been shown to demonstrate some degree of T cell elimination.

Our model excludes the well-known processes of reversible rolling and irreversible adhesion of T cells, due to the lack of sufficient in vitro data to estimate the parameters related to these processes with confidence. Consequently, lymphocytes extravasation through the endothelial capillary wall into the tissues is characterized in our model using a first order process termed as the transmigration rate. Each tissue was considered to have a unique transmigration rate due to the differences in endothelial surface area and chemokine stimuli. However, going forward it might be valuable to augment the model with experimentally observed values of T cell extravasation and endothelial cell interaction (Simionescu et al., 1974; Hamann and Rebstock, 1993; Knust et al., 2009), which can enable the PBPK model to *a priori* predict T cell PK in other species. At present it is very challenging to incorporate such values due to lack of quantitative in

vitro experiments reported in the literature for transmigration rate of lymphocytes for each tissue.

In summary, our results provide an unprecedented insight into whole-body disposition of exogenously administered T cells. Immediately after the administration T cells disappear from the blood, and spleen, liver, lung, kidney, bone, and lymph nodes accounted for more than 90% of T cells in the body. There was no difference found between the PK of T cells in TDLN and IGLN. Interestingly, we did not find T cell accumulation in the solid tumor, however, these observations may differ for targeted T cell like TCR-T and CAR-T cells. Our results suggest that T cell based therapies may be more successful in treating cancers of the lymphatic system and bone marrow metastases compared to solid tumors. It was also found that when T cells are activated against tumor antigens they may accumulate in the lungs at a higher level. The PK data generated in this manuscript was also mathematically characterized using a novel PBPK model developed for exogenously administered T cells. The data and PBPK model presented here also paves the way for the development of a 'systems pharmacokinetic model' for T cells, which can be further combined with the PK model of monoclonal antibody (Shah and Betts, 2012) to develop translational PK models for T cell engaging and targeting antibodies.

ACKNOWLEDGEMENTS

Authors would like to thank Peter Bloomingdale for careful review of the manuscript.

AUTHORSHIP CONTRIBUTIONS

Participated in research design: Khot, Matsueda, Koya and Shah

Conducted experiments: Khot, Matsueda and Thomas

Contributed in developing analytical techniques: Khot and Shah

Performed data analysis: Khot and Shah

Wrote or contributed to the writing of the manuscript: Khot, Koya and Shah

REFERENCES

Ager A, Watson HA, Wehenkel SC, and Mohammed RN (2016) Homing to solid cancers: a vascular checkpoint in adoptive cell therapy using CAR T-cells. *Biochem Soc Trans* **44:**377-385.

Bainbridge DR, Brent L, and Gowland G (1966) Distribution of allogeneic 51Cr-labelled lymph node cells in mice. *Transplantation* **4:**138-153.

Defilippi P, Silengo L, and Tarone G (1993) Regulation of adhesion receptors expression in endothelial cells. *Curr Top Microbiol Immunol* **184:**87-98.

Ganusov VV and Auerbach J (2014) Mathematical modeling reveals kinetics of lymphocyte recirculation in the whole organism. *PLoS Comput Biol* **10:**e1003586.

Girard JP and Springer TA (1995) High endothelial venules (HEVs): specialized endothelium for lymphocyte migration. *Immunol Today* **16:**449-457.

Gowans JL and Knight EJ (1964) The Route of Re-Circulation of Lymphocytes in the Rat. *Proc R Soc Lond B Biol Sci* **159:**257-282.

Gross G and Eshhar Z (2016) Therapeutic Potential of T Cell Chimeric Antigen Receptors (CARs) in Cancer Treatment: Counteracting Off-Tumor Toxicities for Safe CAR T Cell Therapy. *Annu Rev Pharmacol Toxicol* **56:**59-83.

Hall J (1985) The study of circulating lymphocytes in vivo: a personal view of artifice and artifact. *Immunol Today* **6:**149-152.

Hamann A, Klugewitz K, Austrup F, and Jablonski-Westrich D (2000) Activation induces rapid and profound alterations in the trafficking of T cells. *Eur J Immunol* **30:**3207-3218.

Hamann A and Rebstock S (1993) Migration of activated lymphocytes. *Curr Top Microbiol Immunol* **184:**109-124.

Hersey P (1971) The separation and 51 chromium labeling of human lymphocytes with in vivo studies of survival and migration. *Blood* **38:**360-371.

Heslop BF and Hardy BE (1971) The distribution of 51Cr-labeled syngeneic and allogeneic lymph node cells in the rat. *Transplantation* **11:**128-134.

Hogg N (1993) A model of leukocyte adhesion to vascular endothelium. *Curr Top Microbiol Immunol* **184:**79-86.

Knust J, Ochs M, Gundersen HJ, and Nyengaard JR (2009) Stereological estimates of alveolar number and size and capillary length and surface area in mice lungs. *Anat Rec (Hoboken)* **292:**113-122.

Koya RC, Mok S, Otte N, Blacketor KJ, Comin-Anduix B, Tumeh PC, Minasyan A, Graham NA, Graeber TG, Chodon T, and Ribas A (2012) BRAF inhibitor vemurafenib improves the antitumor activity of adoptive cell immunotherapy. *Cancer Res* **72:**3928-3937.

Lechner MG, Karimi SS, Barry-Holson K, Angell TE, Murphy KA, Church CH, Ohlfest JR, Hu P, and Epstein AL (2013) Immunogenicity of murine solid tumor models as a defining feature of in vivo behavior and response to immunotherapy. *J Immunother* **36:**477-489.

Li Z, Krippendorff BF, Sharma S, Walz AC, Lave T, and Shah DK (2016) Influence of molecular size on tissue distribution of antibody fragments. *MAbs* **8:**113-119.

McMillan R and Scott JL (1968) Leukocyte labeling with 51-Chromium. I. Technic and results in normal subjects. *Blood* **32:**738-754.

Melder RJ, Munn LL, Stoll BR, Marecos EM, Baxter LT, Weissleder R, and Jain RK (2002) Systemic distribution and tumor localization of adoptively transferred lymphocytes in mice: comparison with physiologically based pharmacokinetic model. *Neoplasia* **4:**3-8.

Milik AM, Buechner-Maxwell VA, Sonstein J, Kim S, Seitzman GD, Beals TF, and Curtis JL (1997) Lung lymphocyte elimination by apoptosis in the murine response to intratracheal particulate antigen. *J Clin Invest* **99:**1082-1091.

Newick K, O'Brien S, Moon E, and Albelda SM (2017) CAR T Cell Therapy for Solid Tumors. *Annu Rev Med* **68:**139-152.

Norelli M, Casucci M, Bonini C, and Bondanza A (2016) Clinical pharmacology of CAR-T cells: Linking cellular pharmacodynamics to pharmacokinetics and antitumor effects. *Biochim Biophys Acta* **1865:**90-100.

Pabst R (1988) The spleen in lymphocyte migration. *Immunol Today* **9:**43-45.

Pandolfi F, Trentin L, Boyle LA, Stamenkovic I, Byers HR, Colvin RB, and Kurnick JT (1992) Expression of cell adhesion molecules in human melanoma cell lines and their role in cytotoxicity mediated by tumor-infiltrating lymphocytes. *Cancer* **69:**1165-1173.

Rannie GH and Donald KJ (1977) Estimation of the migration of thoracic duct lymphocytes to non-lymphoid tissues. A comparison of the distribution of radioactivity at intervals following i.v. transfusion of cells labelled with 3H, 14C, 75Se, 99mTc, 125I and 51Cr in the rat. *Cell Tissue Kinet* **10:**523-541.

Reina M and Espel E (2017) Role of LFA-1 and ICAM-1 in Cancer. *Cancers (Basel)* **9**.

Sanderson CJ (1976) The uptake and retention of chromium by cells. *Transplantation* **21:**526-529.

Shah DK and Betts AM (2012) Towards a platform PBPK model to characterize the plasma and tissue disposition of monoclonal antibodies in preclinical species and human. *J Pharmacokinet Pharmacodyn* **39:**67-86.

Shah DK and Betts AM (2013) Antibody biodistribution coefficients: inferring tissue concentrations of monoclonal antibodies based on the plasma concentrations in several preclinical species and human. *MAbs* **5:**297-305.

Simionescu M, Simionescu N, and Palade GE (1974) Morphometric data on the endothelium of blood capillaries. *J Cell Biol* **60:**128-152.

Smith ME and Ford WL (1983) The recirculating lymphocyte pool of the rat: a systematic description of the migratory behaviour of recirculating lymphocytes. *Immunology* **49:**83-94.

Smith ME, Martin AF, and Ford WL (1980) Migration of lymphoblasts in the rat. Preferential localization of DNA-synthesizing lymphocytes in particular lymph nodes and other sties. *Monogr Allergy* **16:**203-232.

Sprent J (1976) Fate of H2-activated T lymphocytes in syngeneic hosts. I. Fate in lymphoid tissues and intestines traced with 3H-thymidine, 125I-deoxyuridine and 51chromium. *Cell Immunol* **21:**278-302.

Sprent J and Tough DF (1994) Lymphocyte life-span and memory. *Science* **265:**1395-1400.

Springer TA (1994) Traffic signals for lymphocyte recirculation and leukocyte emigration: the multistep paradigm. *Cell* **76:**301-314.

Stekel DJ, Parker CE, and Nowak MA (1997) A model of lymphocyte recirculation. *Immunol Today* **18:**216-221.

Thakur ML (2013) *Radiolabeled Cellular Blood Elements: Pathophysiology, Techniques, and Scintigraphic Applications*. Springer Science & Business Media.

Trickett A and Kwan YL (2003) T cell stimulation and expansion using anti-CD3/CD28 beads. *J Immunol Methods* **275:**251-255.

Wallace PK, Palmer LD, Perry-Lalley D, Bolton ES, Alexander RB, Horan PK, Yang JC, and Muirhead KA (1993) Mechanisms of adoptive immunotherapy: improved methods for in vivo tracking of tumor-infiltrating lymphocytes and lymphokine-activated killer cells. *Cancer Res* **53:**2358-2367.

Westermann J, Sollner S, Ehlers EM, Nohroudi K, Blessenohl M, and Kalies K (2003) Analyzing the migration of labeled T cells in vivo: an essential approach with challenging features. *Lab Invest* **83:**459-469.

Xia AL, Wang XC, Lu YJ, Lu XJ, and Sun B (2017) Chimeric-antigen receptor T (CAR-T) cell therapy for solid tumors: challenges and opportunities. *Oncotarget* **8:**90521-90531.

Xu WL, Li SL, Wen M, Wen JY, Han J, Zhang HZ, Gao F, and Cai JH (2013) Tracking in vivo migration and distribution of antigen-specific cytotoxic T lymphocytes by 5,6-carboxyfluorescein diacetate succinimidyl ester staining during cancer immunotherapy. *Chin Med J (Engl)* **126:**3019-3025.

Zatz MM and Lance EM (1970) The distribution of chromium 51-labelled lymphoid cells in the mouse. A survey of anatomical compartments. *Cell Immunol* **1:**3-17.

Zhu H, Melder RJ, Baxter LT, and Jain RK (1996) Physiologically based kinetic model of effector cell biodistribution in mammals: implications for adoptive immunotherapy. *Cancer Res* **56:**3771-3781.

FOOTNOTES

This work was supported by the Centre for Protein Therapeutics at University at Buffalo. D.K.S is supported by National Institute of General Medical Sciences grant [GM114179] and National Institute of Allergy and Infectious Diseases grant [AI138195].

FIGURE LEGENDS

Figure 1. Schematic of the PBPK model developed to characterize the whole body disposition of T cells in mice. Tissues are arranged and connected in an anatomical manner, by blood flow (black sold lines) and lymph flow (grey dotted lines). Red arrow shows elimination process via lung, and blue arrows show transmigration process in each tissue. The tissue compartments are color codes as following: red is the whole blood compartment; yellow compartments are lymph node compartments; purple compartments are tissues obtaining blood from the liver compartment; blue compartment is liver that receives the blood from hepatic artery and hepatic portal vein (i.e. gut compartments), teal compartments are tissues obtaining blood directly from the whole blood compartment and draining lymph directly into the lymph node compartment; green compartments are tissues with lymphatic fluid draining in to two lymph nodes (TDLN and IGLN); and pink compartment is the tumor compartment with lymphatic fluid draining in to tumor draining lymph node. 'V' denotes vascular sub-compartment, and 'EV' denotes extravascular sub-compartment.

Figure 2. Observed concentration (%ID/gram of tissue) vs time (hours) curves of Cr-51 labeled T cells in blood, tumor and other tissues excised from melanoma-bearing mice. AUC (%ID/gram*hour) and biodistribution coefficient (i.e. tissue:blood AUC ratio) for each tissue is reported.

Figure 3. Comparison of observed and model generated T cell PK profiles for various tissues.

Figure 4. Superimposition of the observed PK of Cr-51 labeled T cells (red) with previously reported studies of In-111 (green) and I-125 labeled (blue) T cells. Closed symbols represent

non-tumor targeting lymphocytes and open symbols represent lymphocytes activated against tumor antigen. Please refer to Table 2 for further information.

JPET Fast Forward. Published on January 8, 2019 as DOI: 10.1124/jpet.118.252858
This article has not been copyedited and formatted. The final version may differ from this version.

Table 1: List of model parameters along with their numerical values and sources.

Parameter	Description (unit)	Estimate	CV%
J_{lung}	Transmigration rate for each tissue (1/hr)	1843.0	15.4
J_{heart}		34.9	17.2
J_{kidney}		87.3	37.9
J_{brain}		1.4	21.2
J_{muscle}		0.5	19.7
J_{bone}		82.6	16.7
J_{tumor}		0.6	18.6
J_{skin}		0.6	18.7
J_{fat}		1.6	18.5
J_{SI}		12.9	17.1
J_{LI}		5.2	18.1
J_{spleen}		114.0	33.8
J_{liver}		126.9	18.9
$J_{pancreas}$		10.0	20.0
J_{other}		86.8	17.7
R_{kidney}	Retention factor	3.9	37.9
R_{spleen}		9.8	34.8
R_{liver}		2.5	18.4
E_{lung}	Elimination rate (1/hr)	0.84	Fixed (Zhu et al., 1996)
F_{tissue}	Fraction of T cells recirculated to lymph node	1	Fixed (assumption)
Q_{tissue}, L_{tissue}, V_{tissue}	Physiological blood flows, lymph flows and tissue volumes for each mouse tissue (ml/hr, ml/hr, ml)		Fixed (Shah and Betts, 2012)
Q_{tumor}	Tumor blood flow (ml/hr)	6	Fixed (Zhu et al., 1996)
V_{tumor}	Tumor volume (ml or g)	0.45	Fixed (radius~3.85mm)

JPET Fast Forward. Published on January 8, 2019 as DOI: 10.1124/jpet.118.252858
This article has not been copyedited and formatted. The final version may differ from this version.

Table 2: Comparison of different biodistribution studies of T cells in mice. Methods of T cell isolation, expansion, and labeling, as well as tissue biodistribution at 20-24 hours are compared.

Study ID	Wallace *et al*. (1993)		Melder *et al*. (2002)		Khot *et al*. (2018)	
Labeling method	I-125 PKH95 labeled T cells		In-111 oxine labeled T cells		Cr-51 labeled T cells	
Preparation of T cells	Splenocytes exposed to 6000 IU/ml IL-2	TILs extracted from MC38 s.c. tumors	Lymphocytes extracted from spleen	Mice sensitized with splenocytes of MCaIV tumor-bearing C3H mice and lymphocytes extracted from spleen	Splenocytes expanded using anti-CD3, anti-CD28 and IL-2	TILs extracted from B16-BL6 s.c. tumors
Tissues listed in descending order of concentrations at 20-24 hours	Spleen	Lung	Spleen	Lung	Spleen	Lung
	Lung	Spleen	Liver	Spleen	Liver	Spleen
	Liver	Liver	Lung	Liver	Lung	Liver
	Skin	Skin	Tumor	Tumor	Kidney	Kidney
	Muscle	Muscle	Heart	Heart	TDLN	Tumor

JPET Fast Forward. Published on January 8, 2019 as DOI: 10.1124/jpet.118.252858
This article has not been copyedited and formatted. The final version may differ from this version.

Figure 1

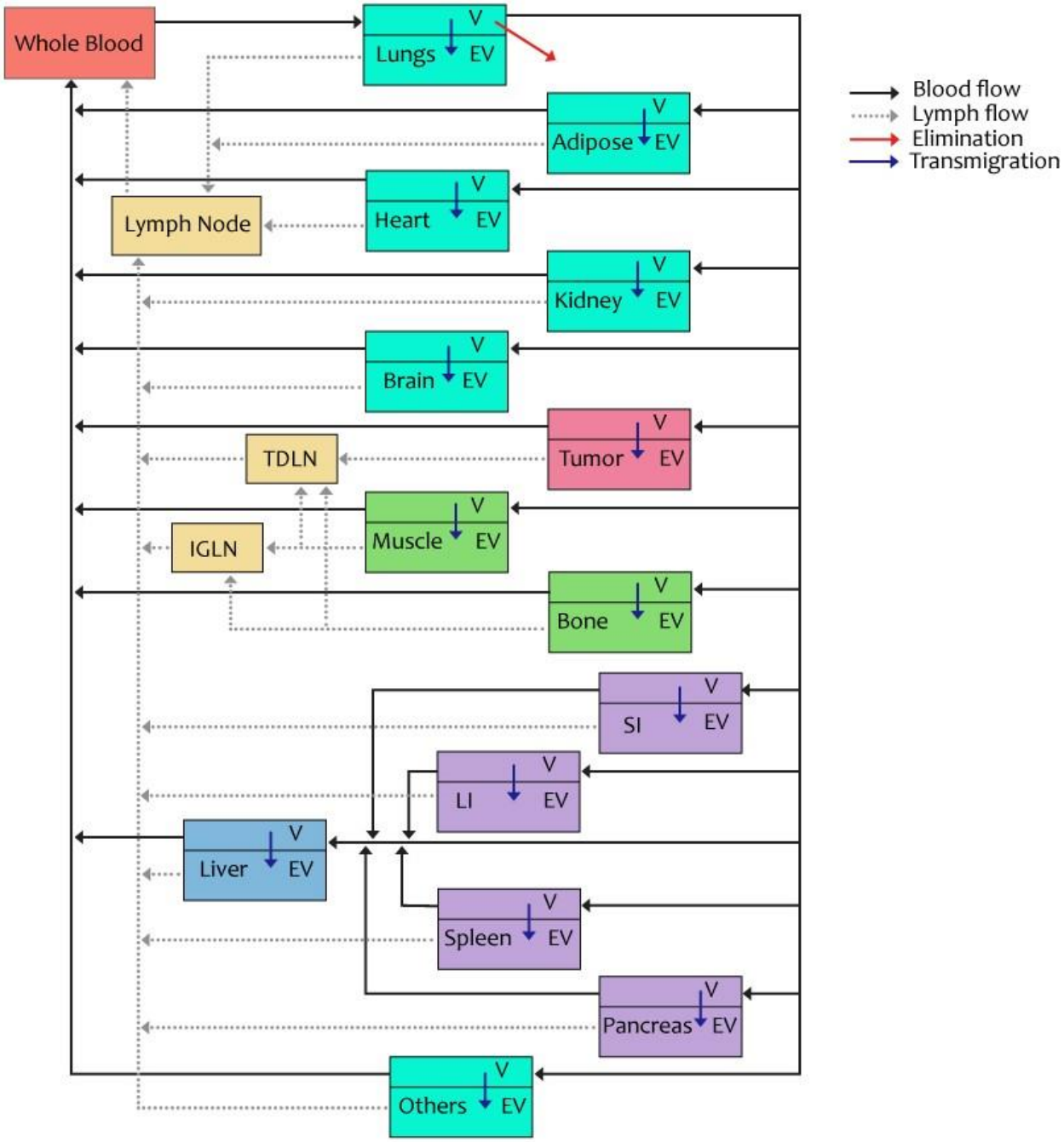

JPET Fast Forward. Published on January 8, 2019 as DOI: 10.1124/jpet.118.252858
This article has not been copyedited and formatted. The final version may differ from this version.

Figure 2

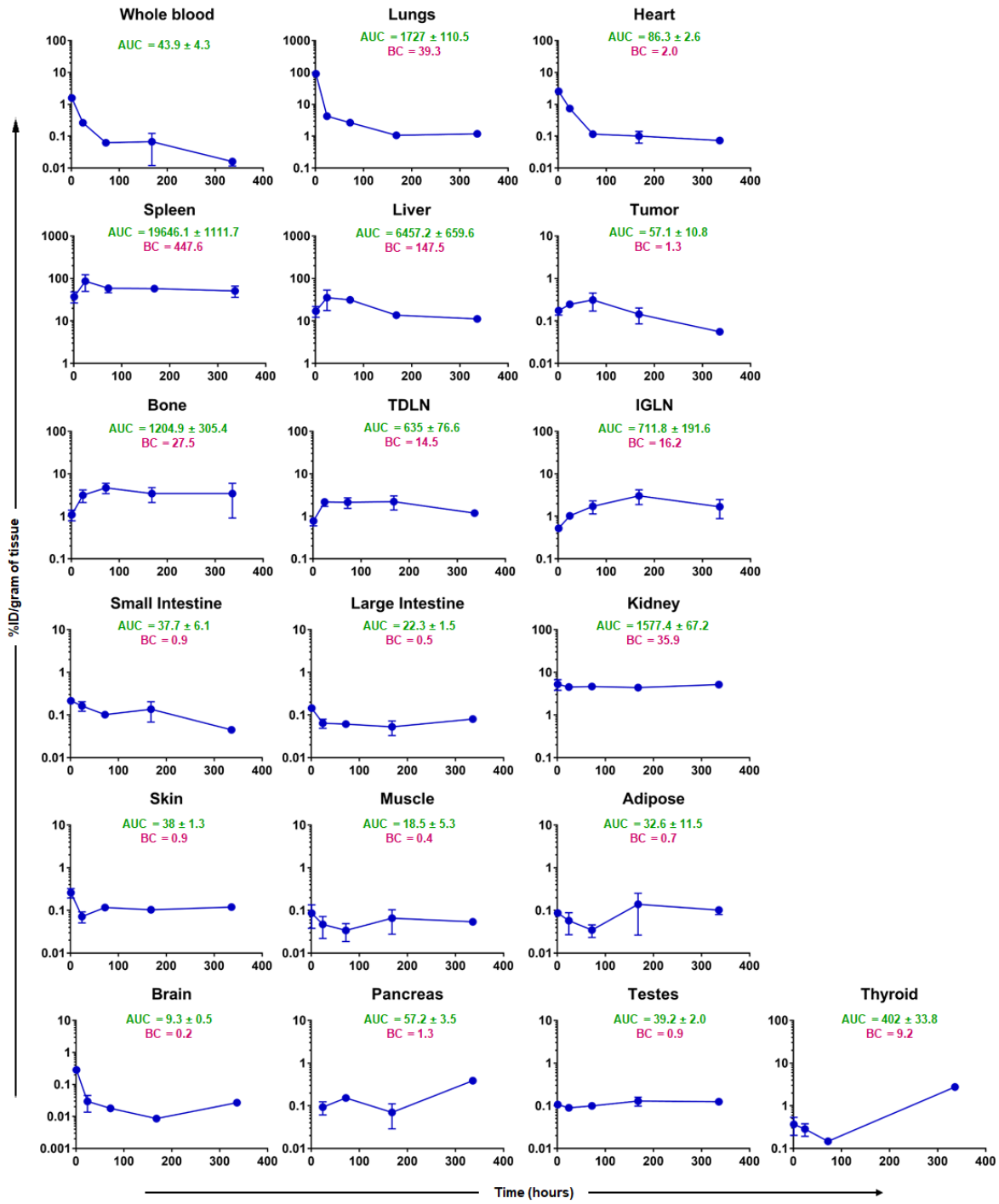

JPET Fast Forward. Published on January 8, 2019 as DOI: 10.1124/jpet.118.252858
This article has not been copyedited and formatted. The final version may differ from this version.

Figure 3

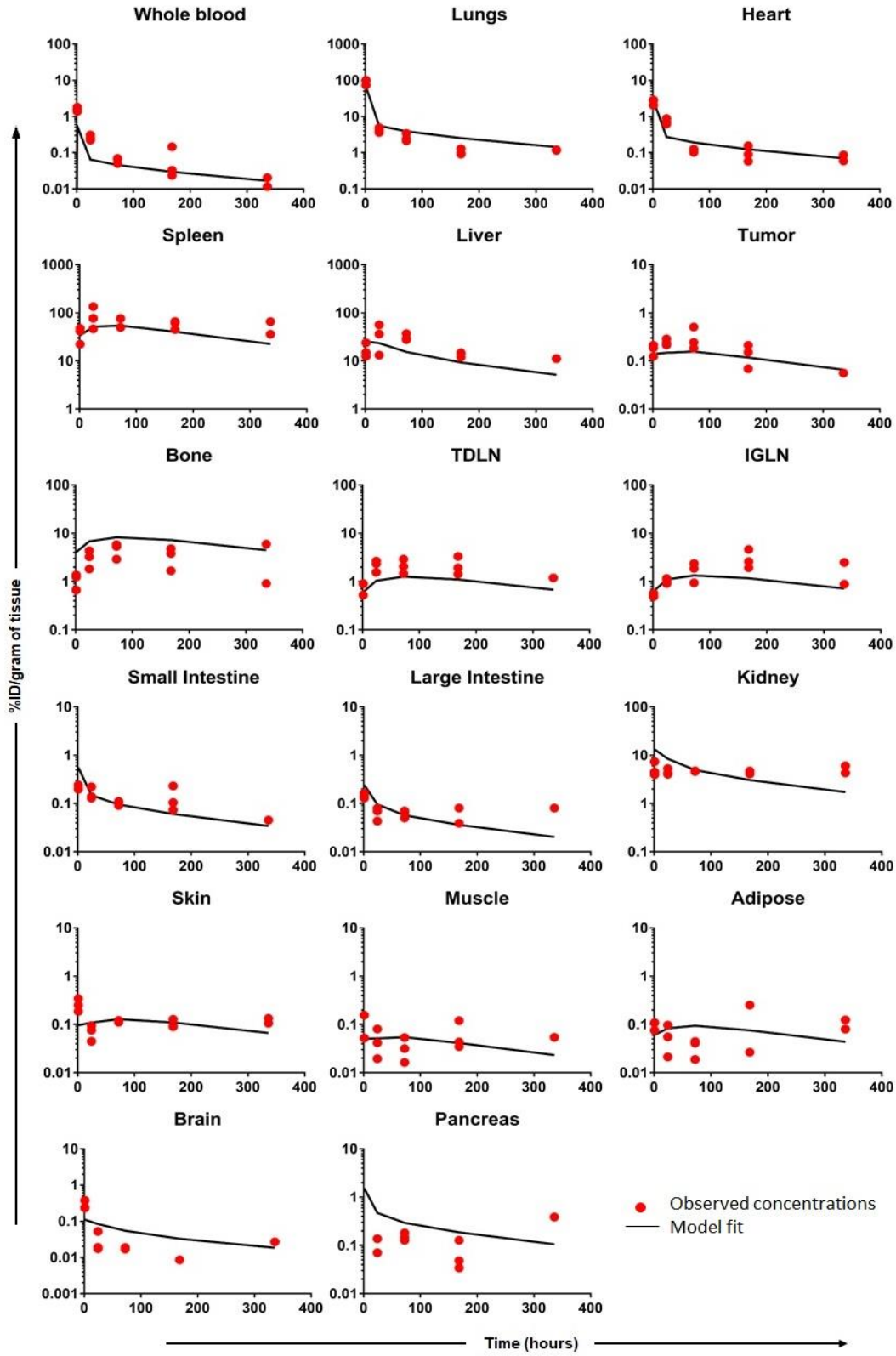

JPET Fast Forward. Published on January 8, 2019 as DOI: 10.1124/jpet.118.252858
This article has not been copyedited and formatted. The final version may differ from this version.

Figure 4